ADVANCED HEALTHCARE MATERIALS
www.advhealthmat.de

Zirconium-Based Metal-Organic Framework Capable of Binding Proinflammatory Mediators in Hydrogel Form Promotes Wound Healing Process through a Multiscale Adsorption Mechanism

UnJin Ryu, Pham Ngoc Chien, Suin Jang, Xuan-Tung Trinh, Hyeon Shin Lee, Le Thi Van Anh, Xin Rui Zhang, Nguyen Ngan Giang, Nguyen Van Long, Sun-Young Nam, Chan Yeong Heo,* and Kyung Min Choi**

The regulation of proinflammatory mediators has been explored to promote natural healing without abnormal inflammation or autoimmune response induced by their overproduction. However, most efforts to control these mediators have relied on pharmacological substances that are directly engaged in biological cycles. It is believed that functional porous materials removing target mediators provide a new way to promote the healing process using their adsorption mechanisms. In this study, the Zr-based metal-organic frameworks (MOF)-808 ($Zr_6O_4(OH)_4(BTC)_2(HCOO)_6$) crystals are found to be effective at removing proinflammatory mediators, such as nitric oxide (NO), cytokines, and reactive oxygen species (ROS) in vitro and in vivo, because of their porous structure and surface affinity. The MOF-808 crystals are applied to an in vivo skin wound model as a hydrogel dispersion. Hydrogel containing 0.2 wt% MOF-808 crystals shows significant improvement in terms of wound healing efficacy and quality over the corresponding control. It is also proven that the mode of action is to remove the proinflammatory mediators in vivo. Moreover, the application of MOF-808-containing hydrogels promotes cell activation, proliferation and inhibits chronic inflammation, leading to increased wound healing quality. These findings suggest that Zr-based MOFs may be a promising drug-free solution for skin problems related to proinflammatory mediators.

1. Introduction

Cytokines, reactive oxygen species (ROS),[1–9] and nitric oxide (NO) are important proinflammatory mediators involved in the wound healing process in multiple-size regimes.[10–13] Manipulation of these multiscale mediators has been shown to play an important role in promoting the wound healing process.[1,2,10–15] While the mediators are necessary, their overproduction makes the healing process slow and often leads to abnormal inflammation and autoimmune response. Specifically, excess production of cytokines causes tissue damage, cellular injury, and chronic inflammation and, in severe cases, can also induce a cytokine storm.[1,2] Moreover, the excess production of nitric oxide and ROS can lead to oxidative stress, inducing cell toxicity and DNA damage. Furthermore, the excess amount of ROS hinders fibroblast migration and proliferation during the generation of the dermal skin layer.[16,17] Thus, there is a need for a strategy to control the mediators and thus promote the

U. Ryu[+]
Industry Collaboration Center
Sookmyung Women's University
Seoul 04310, Republic of Korea

The ORCID identification number(s) for the author(s) of this article can be found under https://doi.org/10.1002/adhm.202301679

[+]Present address: School of Chemical and Biomolecular Engineering, Georgia Institute of Technology, 311 Ferst Dr NW, Atlanta, GA 30332, USA

[++]Present address: Korean Institute of Nonclinical Study, H&Bio. co. Ltd., Seongnam 13620, Republic of Korea

DOI: 10.1002/adhm.202301679

P. N. Chien[++], X.-T. Trinh, L. T. Van Anh, X. R. Zhang, N. N. Giang, N. Van Long, S.-Y. Nam, C. Y. Heo
Department of Plastic and Reconstructive Surgery
Seoul National University Bundang Hospital
Seongnam 13620, Republic of Korea
E-mail: 99261@snubh.org lionheo@snu.ac.kr

S. Jang, K. M. Choi
Department of Chemical and Biological Engineering & Institute of Advanced Materials & Systems
Sookmyung Women's University
Seoul 04310, Republic of Korea
E-mail: kmchoi@sookmyung.ac.kr

H. S. Lee
R&D Center
LabInCube Co. Ltd.
Cheongju 28116, Republic of Korea

wound healing process without the side effects. Previous studies aimed to address this issue have focused on pharmacological mechanisms using active ingredients, such as drugs, antibiotics, or extracts.[3–5] However, these active ingredients directly engage the specific biological cycle related to the inflammatory mediators[3–6] and wound recovery,[7–9] which could induce unexpected effects and drug resistance in their long-term use. Therefore, it is challenging to control mediators without using substances that are directly engaged in the biological cycles. Porous materials, such as clay and minerals, have been used to absorb fluids, exudates, and bacteria to enhance wound healing performance. However, they have not been targeted to control multiscale inflammatory mediators.[18,19] We believe that functional porous materials that can adsorb multiscale target mediators through adsorption or absorption will provide vast opportunities in terms of changing the ways of healing process from a pharmacological mechanism to a multiscale adsorption mechanism inducing fast wound healing process without side effects and drug resistance.

Metal-organic frameworks (MOFs) are porous and reticular materials constructed by coordination bonding between metal oxide units and organic linkers.[20–22] MOFs are known to have chemical and electrostatic interactions both inside of pores and outside of their particles.[23–25] Therefore, MOFs have been shown to have the ability to absorb or adsorb target species in a broad range of gases, molecules, ionic substances, and proteins.[26–30] In previous studies, MOFs have mostly been applied during the wound healing process as carriers for therapeutic drugs or gases by exploiting their intrinsic micropores.[31,32] In some cases, compartments of MOFs have been applied as specific functional materials to engage in a single ingredient, such as ROS, but our study showed a multiscale adsorption mechanism for the removal of multiple proinflammatory mediators involved in the wound healing process.[33–36]

In this study, we focus on the use of the intrinsic properties of MOFs to control the amount of proinflammatory mediators in the wound area inducing fast wound healing performance. Specifically, we chose zirconium-based MOF-808 crystals to control the amount of multiscale proinflammatory mediators involved in wound healing. The robust structural integrity of MOF-808, even in aqueous environments, renders it a safe and practical choice for use in living organisms. Furthermore, our chemical and in vitro affinity assessment underscore MOF-808's ideal pore structure, electrostatic properties, and open metal sites, making it highly efficient in removing proinflammatory mediators, including reactive oxygen species (ROS), nitric oxide (NO), and cytokines. These proinflammatory mediators play pivotal roles in the wound healing process, and MOF-808's capabilities in manipulating them are critical for addressing this challenge.

In addition, we mixed MOF-808 crystals into polyacrylic acid (PAA)-based hydrogels for histological assessment of wound healing in rat skin wound models. Hydrogels are commonly used matrices for wound dressings due to their high water content, biocompatibility, and mechanical characteristics similar to native tissue microenvironments.[37] Importantly, PAA are FDA-approved, cost-effective, and biocompatible polymers.[38] The electrostatic interactions between PAA and MOF-808 ensure the stable integration of MOF-808 crystals within the hydrogel structure and the environment in which MOF-808 functions when applied to wounds.[39]

The hydrogel with 0.2% MOF-808 showed the fastest healing performance, with about 200% improvement in wound healing efficacy over that of the corresponding control. The wound width, re-epithelialization, and collagen density were enhanced by 160.7%, 264.6%, and 132.2%, respectively, compared to the control, following treatment with hydrogels containing 0.2% MOF-808. We also proved that the promotion of wound healing was induced by the in vivo removal of cytokines, ROS, and NO in wound tissues by MOF-808. Additionally, the levels of wound healing factors essential for the functions of mesenchymal cells (vimentin), myofibroblast cells (α-SMA), cellular proliferation (Ki-67), and macrophages (CD68 and F4/80) were improved in the presence of MOF-808.

This is a novel approach in wound healing treatment, in which the specific healing mechanism based on intrinsic adsorption properties of porous materials was proposed, instead of the conventionally direct engagement of bioactive compounds.

2. Results and Discussion

2.1. Structure, Synthesis, and Characterization of MOF-808

The zirconium-based MOF-808 constructed by linking $Zr_6O_4(OH)_4(\text{-}CO_2)_6$ metal cluster with six trimesic acid (H_2BTC) linkers (**Figure 1a**).[40] We chose to use MOF-808 because it has a stable structure and a high number of adsorption sites for proinflammatory mediator removal (Figure 1b).[41–45] The open metal sites on the zirconium clusters of MOF-808 serve as positively charged binding sites for NO derivatives, while the hydroxyl groups present on the clusters stabilize ROS. Moreover, the surface charge of MOF-808 crystals[46–48] could be employed to capture charged cytokines produced in the wound area. The size of pores in MOF-808 is 1.8 nm with an aperture of 1.4 nm in diameter, which can serve as a pathway for NO derivatives and ROS to diffuse into the MOF crystals[40] while remaining the cytokines outside to interact with the surface charge of the crystals (Figure 1b). Given these intrinsic features of MOF-808 crystals, we hypothesized that MOF-808 may be able to adsorb NO, cytokines, and ROS in the wound area (Figure 1c).

For the preparation of MOF-808, it was synthesized by combining a solution of trimesic acid in dimethyl formamide (DMF) with a solution of $ZrOCl_2$ in DMF/formic acid followed by placing the solution in a 130 °C oven for 2 days (Figure S1a, Supporting Information). The powder product was collected and washed with DMF, water, and acetone three times each. In the SEM images, the obtained crystals showed the identical octahedral geometry of MOF-808 with a particle size of 1 μm (Figure S1b, Supporting Information). The powder X-ray diffraction (XRD) pattern was consistent with that of simulated MOF-808, demonstrating that they have the same crystal structure (Figure S1c,

X. R. Zhang, C. Y. Heo
Department of Plastic and Reconstructive Surgery
College of Medicine
Seoul National University
Seoul 03080, Republic of Korea

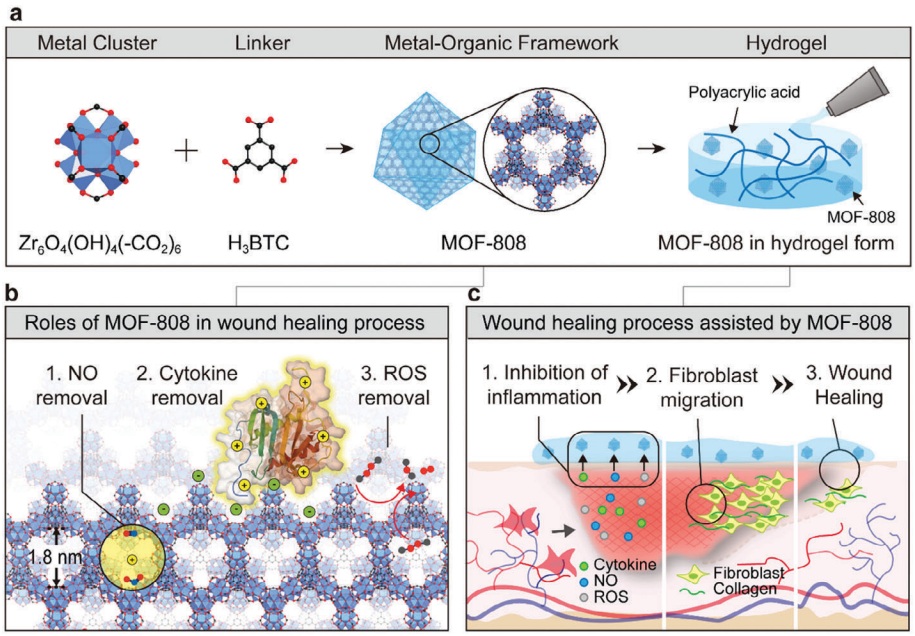

Figure 1. Schematic illustrating MOF-808 synthesis, preparation, and proposed role in the wound healing process. a) The synthesis of MOF-808 and the preparation of MOF-808 into a hydrogel (red: Oxygen, black: Carbon, blue polyhedron: Zr-oxide cluster). b) Removal of proinflammatory mediators (NO, cytokines, ROS) using MOF-808 crystal (red: Oxygen, gray: Hydrogen, blue: Nitrogen). c) The postulated wound healing process promoted by MOF-808 crystals.

Supporting Information).[40] Moreover, the sharp and intense XRD peaks indicated that the product has high crystallinity. The permanent porosity of MOF-808 was measured by nitrogen sorption at 77 K, and the pore size was found to be 1.77 nm (Figure S1d,e, Supporting Information). The stability of MOF-808 in a biological environment was tested in phosphate-buffered saline (PBS), which is a balanced salt solution that is commonly used in biological applications. SEM and XRD analysis of MOF-808 crystals revealed no significant changes in their crystal morphology or structure after placing them in PBS solution for 1, 3, or 7 days (Figure S1b,c, Supporting Information). Cytotoxicity tests were performed to assess the fibroblast proliferation induced by MOF-808 by measuring the cell number or growth before and after exposure to different concentrations of MOF-808 for 24 and 48 h (Figure S1f, Supporting Information), and the results indicated that the MOF-808 prepared in this study is nontoxic when the concentration is up to 10 μg mL^{-1} (Figure S1g, Supporting Information). Taken together, these results verify that we prepared biostable, nontoxic MOF-808 crystals, which could then be tested for their ability to remove proinflammatory mediators.

2.2. Removal of Proinflammatory Mediators Using MOF-808

2.2.1. NO Removal by MOF-808 Crystals

Nitric oxide is a molecule present in aqueous media as its derivatives, including nitrite (NO_2^-) and nitrate (NO_3^-), with sizes ranging from 0.1–0.2 nm.[13,49] MOF-808 contains positively charged sites in its pores, which are favorable for attracting negatively charged NO derivatives.[29,50,51] Therefore, it was expected that the pores of MOF-808 could adsorb NO derivatives using a charge-specific regulatory mechanism (**Figure 2a**).

To confirm that the MOF-808 prepared in this study functioned as expected, we tested the NO removal activity of MOF-808 by using sodium nitrite ($NaNO_2$) and lipopolysaccharide (LPS)-generated cellular NO as representative examples of chemical and biological NO derivatives, respectively. To examine chemical nitrite adsorption by MOF-808, a sodium nitrite solution was treated with MOF-808 crystals. The amount of nitrite remaining in the solution after the MOF-808 was evaluated with the Griess colorimetric assay. The results in Figure 2b show that the pink color from nitrite faded within 30 min after the addition of MOF-808. From the calibration curve (Figure S2a, Supporting Information) and absorbance measurements, it was determined that 0.65 μm nitrite was removed by MOF-808 (10 mg) (Figure 2b and Figure S2b, Supporting Information). In addition, nitrite removal in MOF-808 was also supported by the reduced N_2 uptake after nitrite removal (Figure 2c).

To test that MOF-808 removes cellular NO derivatives, LPS-induced generation was performed in vitro in RAW 264.7 immune cells that are of murine macrophage origin and can therefore produce and secrete inflammatory mediators, including NO and its derivatives. (Figure 2d). After LPS treatment of these cells for 24, 48, and 72 h, MOF-808 crystals were applied to the media at concentrations of 1, 10, and 100 ng mL^{-1}, and the NO derivatives remaining in the media were evaluated with the Griess colorimetric assay (Figure 2e). MOF-808 treatment significantly reduced the concentration of cellular NO derivatives remaining in the growth media regardless of the LPS treatment time; however, the amount of LPS-generated NO removed was dependent on the amount of MOF-808 crystals applied (Figure 2e). Together, the results obtained by applying chemically and biologically induced

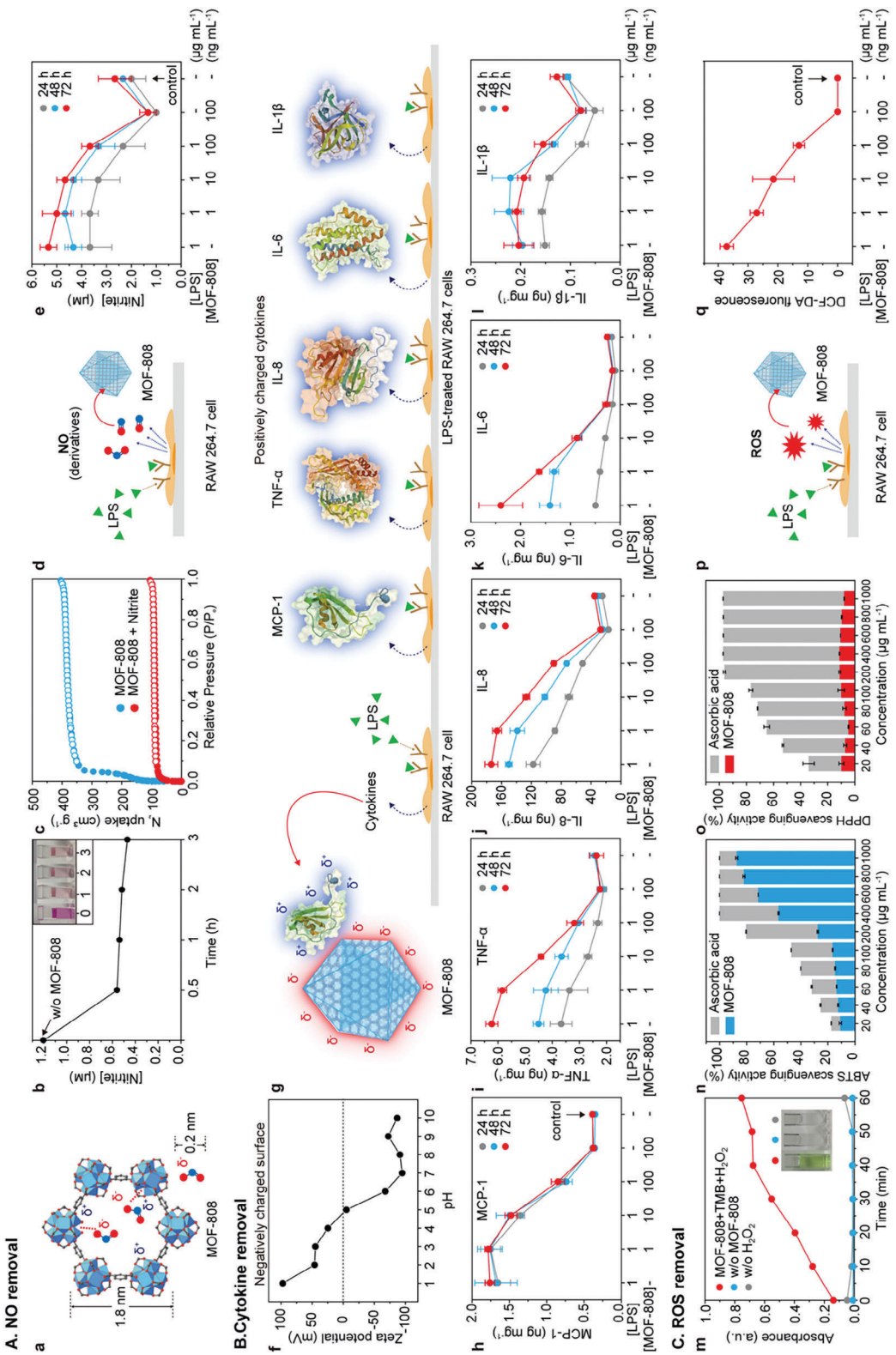

Figure 2. MOF-808 crystals remove proinflammatory mediators. A) NO removal. a) Scheme of the NO derivative (0.1–0.2 nm) removal process by adsorption into the pores of MOF-808 crystals (1.8 nm). b) Nitrite concentration (starting with 1.2 μm $NaNO_2$ solution in the absence of MOF-808) after treatment with MOF-808 for various times (as indicated) and corresponding representative images (inset). c) N_2 uptake by MOF-808 before and after immersion in 35 mM $NaNO_2$ solution. d) Schematic diagram of lipopolysaccharide (LPS)-induced cellular NO production from RAW 264.7 cells and its removal by MOF-808. e) Nitrite concentration after LPS-induced cellular NO production and treatment with 0, 1, 10, or 100 ng mL^{-1} MOF-808

NO derivatives indicate that MOF-808 can decrease NO and its derivatives in wound areas in a dose-dependent manner.

2.2.2. Cytokine Removal by MOF-808 Crystals

Cytokines are proteins of ≈80 kDa (≈2.8 nm) and are typically positively charged.[52–59] As the size of the MOF-808 pore (1.8 nm) would hinder cytokine adsorption, we investigated the surface charge of the MOF-808 crystals. The surface charge was measured by the zeta potential after dispersing MOF-808 crystals in PBS under different pH conditions.[46,60] The MOF-808 crystals exhibited an isoelectric point at pH 4.9 and a negative zeta potential value of −100 mV above pH 7 (Figure 2f), indicating that the surface of the MOF-808 crystals should be negatively charged in a wound environment, which has an alkaline pH value greater than 8.[61] Considering that cytokines are usually positively charged, we hypothesized that the cytokines could adsorb onto the surface of the MOF-808 crystals by electrostatic attraction[62–64] (Figure 2g).

We analyzed the ability of MOF-808 crystals to remove cytokines using five representatives, namely, MCP-1, TNF-α, IL-8, IL-6, and IL-1β, all of which play important proinflammatory roles on wound surfaces. These cytokines were secreted from RAW 264.7 macrophage cells after treatment with LPS (Figure 2g). After the cells were seeded overnight, different amounts of MOF-808 (1, 10, and 100 ng mL^{-1}) were added with 1 μg mL^{-1} LPS for 24, 48, and 72 h. The concentrations of cytokines in the supernatants were measured using ELISA kits, and their concentrations were plotted against that of MOF-808. Cytokine expression increased as the length of LPS treatment increased, and the 72-h treatment group had the highest cytokine expression levels (Figure 2h–l). The MCP-1 concentration was reduced in the presence of MOF-808 (Figure 2h), and the amount of reduction was proportional to the amount of MOF-808 and independent of LPS treatment time. The concentrations of TNF-α (Figure 2i), IL-8 (Figure 2j), IL-6 (Figure 2k), and IL-1β (Figure 2l) varied with LPS treatment time but consistently decreased with increasing amounts of MOF-808 at all treatment times. These results indicate that MOF-808 crystals play an important role in removing inflammatory cytokines from the supernatant and that this effect should be concentration-dependent in wound areas.

2.2.3. ROS Removal by MOF-808 Crystals

ROS are radical species inducing oxidative stress, which can be eliminated by antioxidants having -OH and -OH_2 groups.[65] The Zr-OH(OH_2) metal cluster in the MOF-808 structure contains -OH and -OH_2 groups,[41] which are expected to eliminate ROS in wound areas by reducing them into hydroxide forms and water. We evaluated the antioxidant ability of MOF-808 using chemical (H_2O_2 oxidation, and ABTS and DPPH assays of scavenging activity) and cellular (LPS-stimulated RAW 264.7 cells) approaches. For chemically prepared ROS, H_2O_2 reduction was evaluated in the presence or absence of MOF-808 by measuring the UV–vis absorbance of the tetramethylbenzidine (TMB) colorimetric indicator at 661 nm (Figure 2m). The degree of change in the color of the TMB indicator was related to the degree of ROS stabilization (Figure 2m inset and Figure S3, Supporting Information), and the absorbance at 661 nm increased proportionally from 0.15 to 0.7 over 40 min in the presence of H_2O_2 and MOF-808 (Figure 2m). The ROS removal activity of MOF-808 was also evaluated using ABTS cation radicals and DPPH anion radicals (Figure 2n,o). A clear increase in ABTS scavenging activity with increasing MOF-808 concentration was observed (Figure 2n). On the other hand, DPPH radical scavenging activity was not observed (Figure 2o). We also examined the cellular ROS removal ability of MOF-808 by using RAW 264.7 cells treated with LPS (Figure 2p) and a DCF-DA assay. The amount of ROS present in the RAW 264.7 cells treated with LPS, starting at a value of 35, gradually decreased as the amount of MOF-808 increased (Figure 2q). Together, these results indicated that MOF-808 crystals have a negative surface charge, allowing interactions with positively charged ABTS but not with negatively charged DPPH, and that MOF-808 acts as an antioxidant to control the amount of ROS generated during inflammation in a wound environment.

Previous studies have reported that antioxidants enhance fibroblast migration in wound areas.[16,17] As MOF-808 has antioxidant activity, it was thus expected that MOF-808 would accelerate fibroblast migration. Fibroblast migration was assessed in NIH-3T3 cells as an indicator of wound healing. Cells were grown to confluence, after which a wound was simulated by scratching a line in the middle of the confluent cells in the culture dish. The cells were then further cultured in the presence of different MOF-808 concentrations for 5, 10, and 20 h. The fibroblasts on both sides of the scratch migrated to the center and began to fill in the scratched area (Figure S4a, Supporting Information). Notably, the migration accelerated with increasing MOF-808 dose after 20 h, and the migration area reached a maximum of 85% after treatment with 100 ng mL^{-1} MOF-808 (Figure S4b and Table S1, Supporting Information). This result suggests that the antioxidant activity of MOF-808 could accelerate fibroblast migration in the wound area.

for 24, 48, and 72 h. B) Cytokine removal. f) pH-dependent zeta potential curve of MOF-808 dispersed in PBS. g) Schematic diagram of LPS-induced cellular cytokine (MCP-1, TNF-α, IL-8, IL-6, and IL-1β) production from a RAW 264.7 cells and their removal from the growth media by attraction to the MOF-808 crystal surface. Concentrations of h) MCP-1, i) TNF-α, j) IL-8, k) IL-6, and l) IL-1β were measured by ELISA kits after LPS induction and treatment with 0, 1, 10, or 100 ng mL^{-1} MOF-808 and 1 μg mL^{-1} LPS for 24, 48, and 72 h. C) ROS removal. m) Time-dependent absorbance at 661 nm of TMB with MOF-808-treated H_2O_2 solution (red), H_2O_2 solution only (blue), and MOF-808-treated solution only (gray). n) ABTS scavenging activity (measured at 670 nm) of MOF-808 and ascorbic acid. o) DPPH scavenging activity (measured at 517 nm) of MOF-808 and ascorbic acid. p) Schematic diagram of LPS-induced cellular ROS production from RAW 264.7 cells and its removal by MOF-808. q) DCF-DA fluorescence of LPS-induced cellular ROS treated with 0, 1, 10, or 100 ng mL^{-1} MOF-808 and 1 μg mL^{-1} LPS using a DCF-DA assay. The presented values are the experimental results of the three trials. Data are shown as the mean ± SEM.

2.3. MOF-808 Crystals in a Hydrogel Form Promote Wound Healing

2.3.1. Formation of MOF-808 Containing Hydrogel

To prepare MOF-808 suitable for application to wound areas, we homogeneously dispersed MOF-808 crystals in a PAA-based hydrogel gel. PAA was chosen as a hydrogel-forming agent because it has negative charges in its backbone structure due to the deprotonated carboxylic groups.[66] The PAA backbone mainly interacts with water to form the hydrogel and repels the MOF-808 crystals having a negatively-charged surface, thus making the MOF-808 crystals well dispersed in the hydrogel as represented in Figure S5a, Supporting Information. Therefore, the hydrogel having MOF-808 particles can be deposited to form a coating layer on the wound area. The hydrogel was prepared to have 0, 0.1, 0.2, 0.4, 0.6, and 0.8 wt% MOF-808 crystals in the mixture of PAA in water, then subjected to test the wound healing efficacy (Figure S5b, Supporting Information). As the concentration of the MOF-808 crystals increased, the transparent gel became opaque (Figure S5b, Supporting Information). Optical microscopy images showed that MOF-808 particles were evenly dispersed in the hydrogel (Figure S5c, Supporting Information). FT-IR spectral analysis showed that the MOF-808 peaks at 1700 cm^{-1} (C=C stretch), 1400 cm^{-1} (COO symmetric stretch), and 650 cm^{-1} (Zr-O vibration)[67] became sharper and stronger with increasing MOF-808 content (Figure S5d, Supporting Information). The hydrogel containing 0.2 wt% MOF-808 was coated on a glass (Figure S6 second column, Supporting Information). The coating layer was shown to have constant adhesion properties after tilting at 90 ° and 180 ° for 6 h (Figure S6 third and fourth columns, Supporting Information), which indicates that the coated layer is expected to adhere stably to the skin for a long-time during activity. In the evaluation of the long-term stability, the pH, viscosity, and adhesion properties are maintained even after 2 years-accelerated aging process (Table S2 and Figure S6, Supporting Information). The hydrogel containing MOF-808 efficiently reduces the amount of NO, cytokines, and ROS in vitro compared with the hydrogel without MOF-808 (Figures S7 and S8, Supporting Information), which is consistent with the observation for MOF-808 crystals in Figure 2.

The roles and functions of MOF-808 crystals in the wound healing process were shown by comparing the wound healing process for the samples having no and different contents of MOF-808 crystals. Moreover, the function of MOF-808 in the hydrogel for the removal of NO, cytokines, and ROS was proven by in vivo observation of the amount of the proinflammatory mediators before and after the wound healing process.

2.3.2. Wound Healing Efficacy of the MOF-808 Crystals in the Hydrogel

We evaluated the wound healing efficacy of the MOF-808 crystals using a rat skin wound model (**Figure 3**a,b). Sprague Dawley adult male rats were randomly divided into seven groups of 10 rats, with six groups receiving different concentrations of MOF-808 in the hydrogel and one control group. Full-thickness excisional wounds were created using 10 mm biopsy punch-modified tools on the dorsal side of the rats. Hydrogels containing the MOF-808 crystals were applied once a day for 14 days to cover the wound area, and all wound areas were sealed with Tegaderm film (1624 W, 3M, Deutschland GmbH Health Care Business, Germany). The wounds in the control group rats remained untreated. All rats maintained their weight throughout the test period, indicating that the MOF-808 crystals did not cause systemic toxicity (Figure S9, Supporting Information).

The wound area was more effectively reduced in the presence of the MOF-808 crystals than in the control groups of one untreated and another treated with the hydrogel without the MOF-808 crystals (Figure 3b). In particular, the hydrogel with 0.2 wt% MOF-808 crystals showed the fastest recovery rate based on the measured sizes of the wound areas (Figure 3b–e and Table S3, Supporting Information). The remaining wound area decreased to 55%, 62%, and 50%, on average, compared with each control group after 7, 10, and 14 days, respectively. These results indicate that the hydrogel with 0.2 wt% MOF-808 crystals enhances the wound healing efficacy, with about 200% improvement over that of the corresponding control. When the content of MOF-808 crystals is higher than 0.2 wt%, however, the wound healing efficacy was decreased. Considering the concentration-dependent removal behavior observed for NO, cytokines, and ROS (Figure 2), this is because MOF-808 removes the proinflammatory mediators excessively in higher concentration and thus delay the healing process. Comparing results from the control sample and the hydrogel without MOF-808 (the hydrogel with 0 wt% MOF-808 crystals), the PAA hydrogel itself has a minor effect on wound healing efficacy but not as much as MOF-808. The wound healing efficacy of the hydrogel with 0.2 wt% MOF-808 crystals was compared with the recombinant human epidermal growth factor (rh-EGF) containing product using the same rat skin wound model and evaluation method. Surprisingly, it was observed that the hydrogel with 0.2 wt% MOF-808 crystals showed similar wound healing performance with the rh-EGF-containing product (Figure S10, Supporting Information). The efficacy of bacterial prevention for the hydrogel having 0.2 wt% MOF-808 crystals was further investigated by using *Staphylococcus aureus*. The experimental result showed the hydrogel with 0.2 wt% MOF-808 crystals has the ability to prevent bacterial infection (Figure S11, Supporting Information). These results proved that the MOF-808 crystals dispersed in hydrogels efficiently enhance the wound healing efficacy and show the fastest healing performance with 0.2 wt% content.

2.3.3. Histological Assessment of MOF-808 Crystals in the Hydrogel

Histological assessment of the rat skin wounds was performed to confirm the quality of wound healing at the tissue level. Granular tissue formation, epidermis layer construction, and collagen deposition[68] were evaluated by histological analysis of the wound width, re-epithelialization, and collagen density using hydrogels with MOF-808 crystals. Based on a visual assessment of the wound healing performance, hydrogels containing 0 wt%, 0.1 wt%, and 0.2 wt% MOF-808 crystals were chosen for use in this analysis (Figure 3b). Five-micrometer-thick biopsied tissue sections were prepared and stained with hematoxylin and eosin to measure granulation tissue (Figure 3f,g) and the epidermal layer

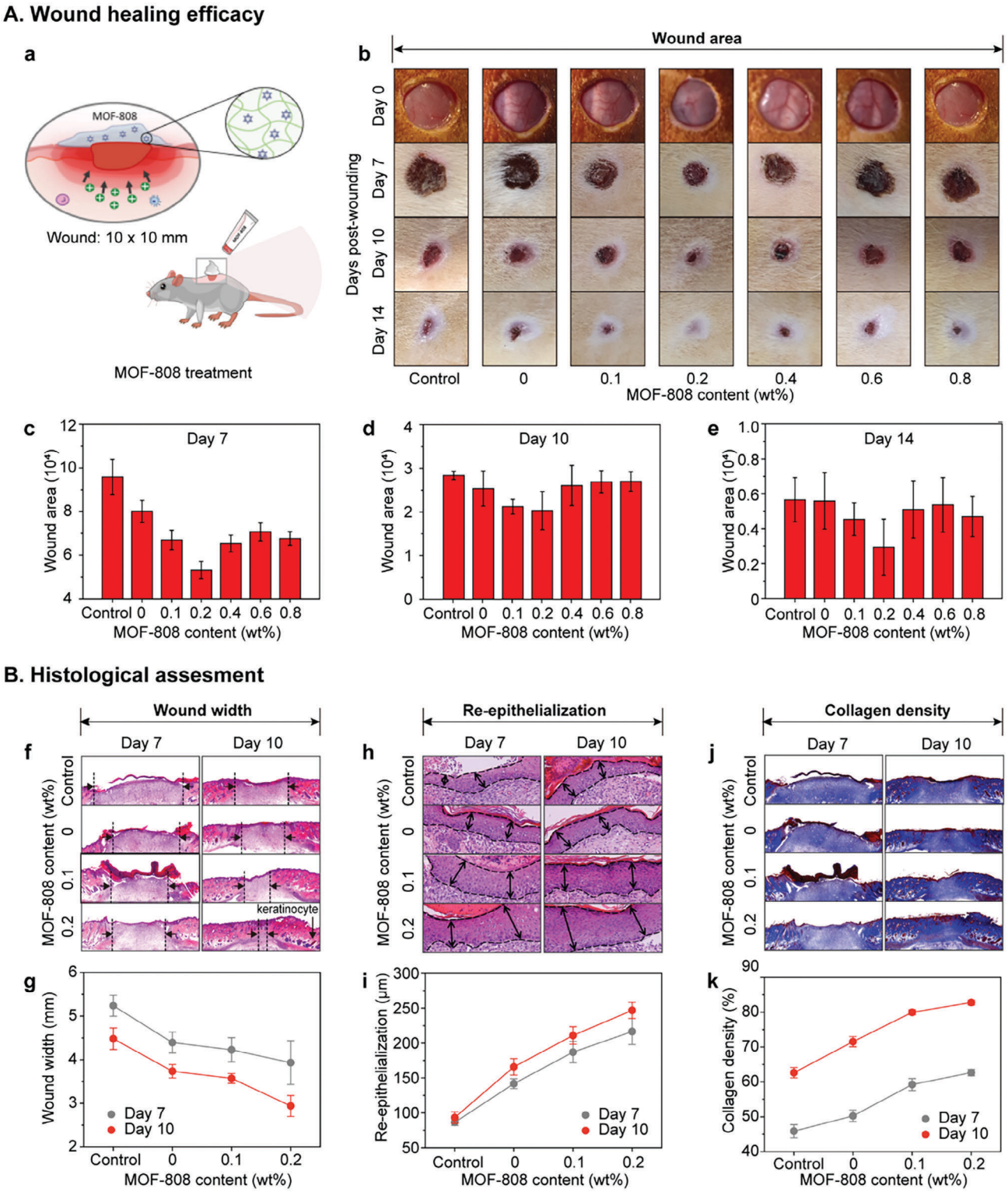

Figure 3. MOF-808 promotes the skin wound healing process. A) Wound healing efficacy. a) Model of MOF-808 treatment in rat skin wound. b) Representative photographs of the control and MOF-808-treated rat skin wounds. Quantification of wound closure presented as wound width on c) days 7, d) 10, and e) 14 after wounding. B) Historical assessment representative. f,h) H&E staining and j) MT staining of wound healing sections on days 7 and 10 after wounding. f) The wound widths are marked with arrows and g) quantified according to the content of MOF-808 crystals. Re-epithelialization shown as h) the thickness of the epithelial tissue is marked with double-sided arrows and i) quantified according to the content of MOF-808 crystals. j) The collagen density is stained blue and k) quantified according to the content of MOF-808 crystals. The presented values are the experimental results on 10 rats for each group. Data are shown as the mean ± SEM. Statistical analysis was carried out using Prism Software.

(Figure 3h,i) and with Masson's trichrome to measure collagen density (Figure 3j,k). All tissue sections were analyzed on day 7 and day 10. The wound width gradually decreased compared to that in the control group with increasing MOF-808 crystal content in the hydrogel (Figure 3f,g, and Figure S12a and Table S4, Supporting Information). After 10 days, the group treated with 0.2 wt% MOF-808 crystals showed a well-organized and uniform wound width with a uniform thickness (Figure 3f) and a wound area that was almost remodeled with keratinocytes (Figure 3f). Moreover, the thickness of the epithelial tissue increased as the MOF-808 crystal content in the hydrogel increased (Figure 3h,i, and Figure S12b and Table S4, Supporting Information). The group treated with 0.2 wt% MOF-808 crystals showed the highest re-epithelialization with complete epithelial tissue, which is expected to prevent scar formation, on day 10. Additionally, Masson's trichrome staining revealed that collagen formation was enhanced by applying MOF-808 crystals (Figure 3j) and that the collagen density increased with increasing MOF-808 crystal content in the hydrogel up to 0.2 wt% (Figure 3j,k, and Figure S12c and Table S4, Supporting Information). These histological results clearly indicated that the wound healing quality was improved in terms of wound width, re-epithelialization, and collagen density, which were enhanced by 160.7%, 264.6%, and 132.2%, respectively, compared to the control.

2.3.4. Proof of Proinflammatory Mediator Regulation in Wound Tissue using Hydrogels Containing MOF-808 Crystals

Given that MOF-808 crystals in hydrogel were shown to increase the efficacy and quality of wound healing, we next sought to assess whether proinflammatory mediators were affected by MOF-808 in these same tissues (**Figure 4**). We analyzed the amounts of NO, ROS, and cytokines in the tissue before and after treatment with hydrogels containing 0, 0.1, and 0.2 wt% MOF-808 crystals. Wound lysates containing proinflammatory mediators on days 7 and 10 were extracted from the tissues by centrifugation. The amount of NO remaining in the lysates was measured with a Griess colorimetric assay, and the antioxidant activity against ROS in the lysates was confirmed with a DCF-DA assay (Figure 4a,b). The concentration of NO gradually decreased as the MOF-808 content increased up to 0.2 wt% (Figure 4a), which is consistent with in vitro observations (Figure 2e). The amount of ROS also gradually decreased with increasing MOF-808 crystal content on days 7 and 10 (Figure 4b), indicating that MOF-808 is an effective antioxidant that can reduce ROS for skin wound recovery. The amount of MCP-1, TNF-α, IL-8, IL-6, and IL-1β existing in the wound tissues were visualized by immunofluorescence (Figure 4c–g), and their quantities in the lysate were determined using ELISAs (Figure 4h–l and Table S5, Supporting Information) or ImageJ software (Figure S13, Supporting Information). The green fluorescence of MCP-1 gradually decreased compared with that of the control group in the presence of MOF-808 crystals (Figure 4c). This trend was also observed for the other 4 cytokines (TNF-α, IL-8, IL-6, and IL-1β) (Figure 4d–g). Moreover, the cytokine quantities in the lysate gradually decreased with increasing MOF-808 crystal content on days 7 and 10 (Figure 4h–l). Comparing results from the control sample and the hydrogel containing 0 wt% MOF-808, PAA in hydrogel also affects the amount of the mediators. However, it is shown in Figure 4 that the concentration of MOF-808 mainly regulates the amount of the mediators remaining in the wound area. These results show that the MOF-808 crystals in the hydrogel removed the proinflammatory mediators (NO, ROS, and cytokines) generated in vivo and in vitro, and we conclude that this promotes wound healing.

2.3.5. Wound Healing Factors Affected by the MOF-808 Crystals

Next, we sought to determine the effects of MOF-808-mediated proinflammatory mediator removal on the quality of the wound healing process by measuring wound healing factors. Vimentin and α-SMA were measured as indicators of mesenchymal and myofibroblast cell activation and Ki-67 was measured as an indicator of cell proliferation. Macrophages (CD68 and F4/80) were also evaluated as an indicator of chronic inflammation inhibition.[69–72] Hydrogels containing 0, 0.1, and 0.2 wt% MOF-808 crystals were applied to rat skin wounds, and the expression of the abovementioned wound healing factors was assessed on days 7 and 10. The immunofluorescence staining images for indicators of the wound tissue were shown in **Figure 5**a–e, and their amounts were quantified according to the green fluorescence intensity (Figure 5f–j and Table S6, Supporting Information). The result of staining was performed using a confocal microscope (Zeiss LMS 710, ZEN software, Germany) and the fluorescence signal was analyzed using ImageJ software. Vimentin, α-SMA, and Ki-67 immunofluorescence increased with increasing MOF-808 crystal content in the hydrogel, indicating that the expression or stability of wound healing factors related to cell migration and proliferation increased in the presence of the MOF-808 crystals (Figure 5a–c,f–h). In contrast, CD68 and F4/80 immunofluorescence decreased with increasing MOF-808 crystal content in the hydrogel (Figure 5d,e,i,j). This indicates that the expression of wound healing factors related to chronic inflammation decreased in the presence of MOF-808 crystals. The impact of MOF-808 on wound vascularization was also monitored by measuring the expression level of CD31 during wound healing.[73] We stained wound healing tissues on days 7 and 10 and then measured the CD31 intensity (Figure S14, Supporting Information). It is observed that the intensity from the hydrogel with 0.2 wt% MOF-808 was higher than those from other samples on days 7 and 10. These results indicate that the hydrogel with 0.2 wt% MOF-808 also promotes the formation of vascularization during the wound healing process. Notably, these trends were linearly proportional to the MOF-808 content, and 0.2 wt% was determined to be the optimal amount of MOF-808 for the wound healing process considering wound healing efficacy (Figure 3). All evidence regarding the in vitro proinflammatory mediator removal (Figure 2) the wound healing efficacy (Figure 3), the in vivo proinflammatory mediator removal (Figure 4), and the wound healing factors (Figure 5) indicated that MOF-808 crystals adsorb proinflammatory mediators to promote the wound healing process by a multiscale regulatory mechanism.

3. Conclusion

In this study, we show that MOF-808 crystals can remove proinflammatory mediators from the immediate area surrounding a

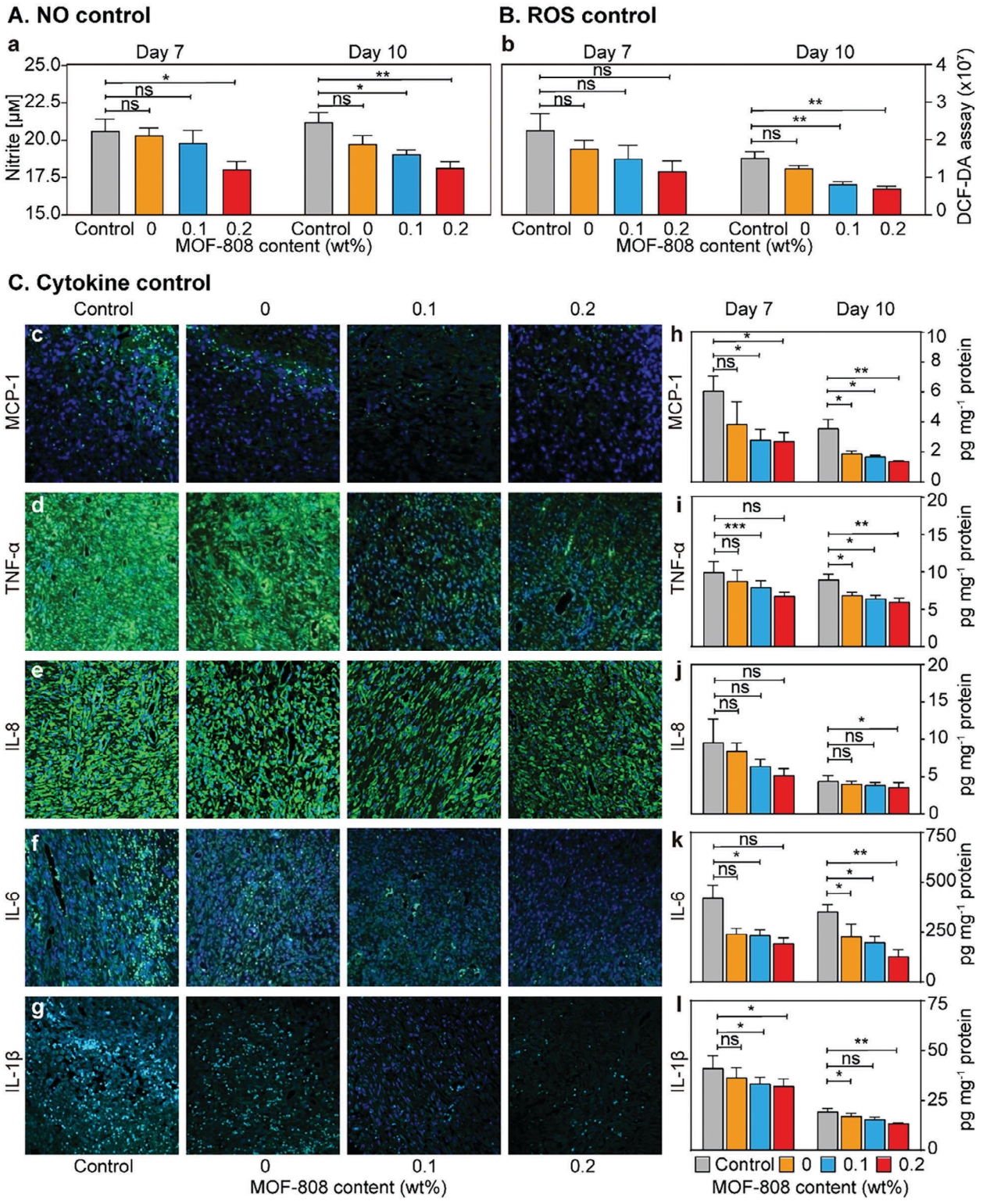

Figure 4. Proinflammatory mediator regulation in wound tissue using hydrogels containing MOF-808 crystals. A) NO control. a) Nitrite concentrations in the control and MOF-808-hydrogel treated groups on days 7 and 10 after wounding. B) ROS control. b) DCF-DA fluorescence in the control and MOF-808-hydrogel treated groups on days 7 and 10 after wounding. C) Cytokine control. c–g) Immunofluorescence (IF) microscopy of c) MCP-1-, d) TNF-α-, e) IL-8-, f) IL-6-, and g) IL-1β -stained wound tissues on day 7 (green). Nuclei were counterstained with DAPI (blue). h–l) The concentrations of h) MCP-1, i) TNF-α, j) IL-1β, k) IL-6, and l) IL-8 in the control and MOF-808-hydrogel treated groups on days 7 and 10 after wounding as determined by ELISA. The presented values are the experimental results on 10 rats for each group. Five IF staining images were taken for each sample in groups. Data are shown as the mean ± SEM. ^{ns} $p \geq 0.05$, * $p < 0.05$, ** $p < 0.005$, *** $p < 0.001$. Statistical analysis was carried out using Prism Software.

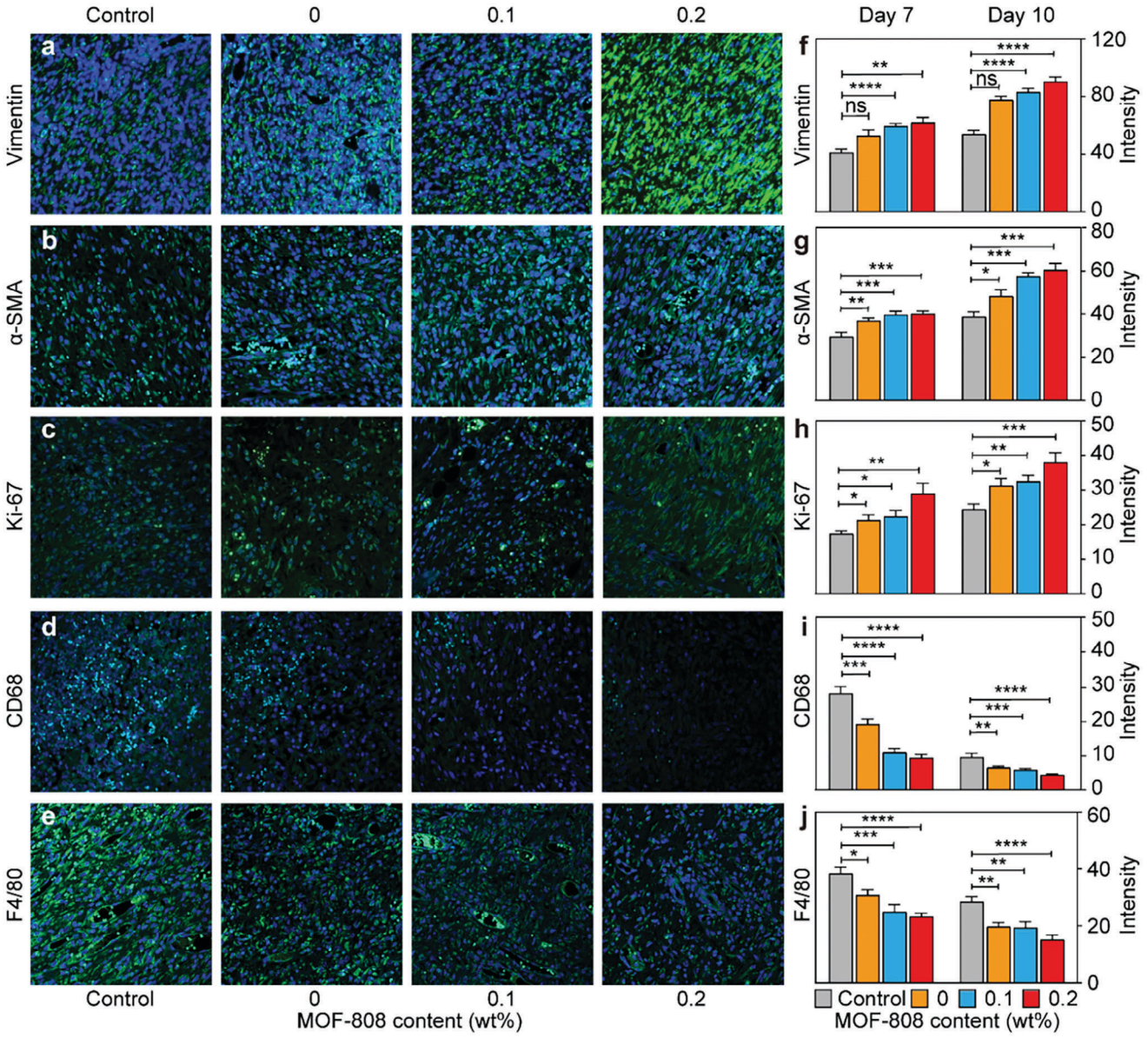

Figure 5. Wound healing factors affected by the MOF-808 crystals. Immunofluorescence (IF) microscopy of a) vimentin-, b) α-SMA-, c) Ki-67-, d) CD68-, and e) F4/80-stained wound tissues on day 7 (green). Nuclei were counterstained with DAPI (blue). The concentrations of f) vimentin, g) α-SMA, h) Ki-67, i) CD68, and j) F4/80 in the control and MOF-808-hydrogel treated groups on days 7 and 10 after wounding determined by quantifying the green intensity of fluorescence signal by using ImageJ software. The presented values are the experimental results on 10 rats for each group. Five IF staining images were taken for each sample in groups. Data are shown as the mean ± SEM. ^{ns} $p \geq 0.05$, * $p < 0.05$, ** $p < 0.005$, *** $p < 0.001$. Statistical analysis was carried out using Prism Software.

wound, leading to the promotion of the wound healing process. It was suggested that MOF-808 crystals have an intrinsic ability to bind NO, cytokines, and ROS induced by both chemical and biological pathways. Dispersal of MOF-808 crystals in hydrogel form and application of this hydrogel to rat skin wounds revealed that the wound healing effects, as indicated by wound width, re-epithelialization, and collagen density, were the fastest after treatment with the hydrogel containing 0.2 wt% MOF-808 crystals. In vivo analysis using tissues obtained from rat skin wounds showed that the improved wound healing performance could be attributed to the removal of NO, cytokines, and ROS proinflammatory mediators from the wound area. Moreover, our results showed that MOF-808 could affect the levels of wound healing factors involved in the promotion of cell activation and proliferation, and the inhibition of chronic inflammation at the wound site, leading to enhanced quality of the wound healing process. This study provides the first case of using MOFs for regulating proinflammatory mediators in the wound healing process and needs further studies revealing precise mechanisms for cell migration and proliferation as well as confirming the efficacy and safety in diverse applications including a diabetic rodent wound model.

4. Experimental Section

Preparation of MOF-808 Crystals: The MOF-808 was prepared via a typical solvothermal synthesis that was modified from a reported method.[32] Ligand solution was prepared by dissolving H_3BTC (5 mmol, 1 g) in DMF (112.5 mL). Separately, a metal solution was prepared by dissolving $ZrOCl_2 \cdot 8H_2O$ (15 mmol, 4.85 g) in DMF (112.5 mL) with formic acid (225 mL). The ligand and metal solution were combined in a 500 mL Nalgene bottle and placed in an oven at 130 °C for 2 days. The powder product was separated using a centrifuge (6000 rpm for 10 min) followed by washing with DMF, water, and acetone. Each washing solvent was rinsed with MOF-808 crystals three times a day for 3 days. After washing, the product was dried by a freeze dryer to get the fine powder.

Cell Toxicity Test: NIH-3T3 cells were used to examine the cytotoxicity of MOF-808 to confirm that the MOF-808 was not harmful to cells. NIH-3T3 cells with a concentration of 4×10^4 cells mL^{-1} were seeded into a 24-well plate, then cells were treated with different concentration of MOF-808 such as 0.1 and 1 µg mL^{-1} and grew for 24, 48, and 72 h at 37 °C, 5% CO_2. Cell viability was quantified by using an MTT assay. Briefly, after incubation of different MOF-808 concentrations for 24, 48, and 72 h, cells were treated with 5 µg mL^{-1} of MTT final concentration by incubation at 37 °C, 5% CO_2 for 4 h. After that media was removed, and purple cell pellets were dissolved in DMSO by incubation at room temperature for 10 min. Cell viability was calculated through optical density at 570 nm.

Determination of Chemically Induced NO Removal Activities of MOF-808: The NO removal activity of MOF-808 was measured by using a Griess reagent with sodium nitrite ($NaNO_2$). The Griess solution was prepared by mixing the Griess reagent (0.8 g, Aldrich) and distilled water (20 mL). The experiment was performed by increasing the treatment time of nitrite while fixing the concentration of MOF-808 and nitrite solution. A total of 1.5 mL of nitrite solution (1.2 µM) was added to MOF-808 (10 mg) and kept in a vial. After a period of time had elapsed, MOF-808 was removed using a syringe filter with a 0.45 µm pore size. An equal volume (1.5 mL) of Griess solution and the filtered nitrite solution were mixed in a disposable cuvette and read the absorbance at 540 nm after 15 min. The amount of nitrite absorbed by MOF-808 was calculated from the sodium nitrite standard curve.

Determination of Chemically Induced H_2O_2 Removal Activities of MOF-808: The H_2O_2 scavenging activity of MOF-808 was measured by using TMB photometric measurement that was modified from a reported method.[41] The reaction solution was prepared by dissolving TMB in ethanol and dispersing MOF-808 in distilled water by ultrasonication, respectively. The experiment was performed by increasing the treatment time while fixing the concentration of MOF-808 and TMB solution, and the experiment in the absence of each MOF-808 and H_2O_2 was used as a control. In the typical method, 200 µL of TMB (5 mM), 1.5 mL ethanol, 1.5 mL MOF-808 solution (10 mg mL^{-1}), 100 µL of distilled water, and 100 µL of H_2O_2 (500 mM) were added sequentially in 10 mL vial. The mixture was reacted at 40 °C with a stirring speed of 200 rpm for different reaction times at 10-min intervals. After a certain reaction time, the mixture was immediately filtered by a syringe filter. The absorbance of the resultant solution was measured wavelength from 550 to 750 nm at room temperature, and the absorbance at 661 nm was used for relative quantity analysis of H_2O_2 removal against TMB oxidation analysis by antioxidant activity.

Measurement of Cytokine Production on Cells by ELISA: The effect of MOF-808 on cytokine levels was investigated by LPS-treated cells. The RAW264.7 cells (2.5×10^5 cells mL^{-1}) were seeded into a 24-well plate overnight and then pretreated with different concentrations of MOF-808 of 1, 10, and 100 ng mL^{-1} for 1 h prior to 24, 48, and 72 h treatment with 1 µg mL^{-1} of LPS in 37 °C, 5% CO_2 incubator. Subsequently, cell-free supernatants were collected and stored at −20 °C for cytokine assays. The concentration of MCP-1, TNF-α, IL-8, IL-6, and IL-1β in the culture supernatant was measured using ELISA kits purchased from BD Biosciences and Mybiosource, SD, USA. The absorbance was measured at 450 nm using EPOCH2 microplate spectrophotometer (Agilent, CA, USA).

Measurement of NO on Cells: The cell-free supernatants collected from the above step were also used for NO measurement. The Griess-modified reagent was used for measuring NO oxidation products on cells. A volume of 100 µL of the Griess-modified reagent was mixed with 100 µL of the supernatants. The mixtures were incubated at room temperature for 15 min. Nitrite standard solutions of 0, 1.6125, 3.125, 6.25, 12.5, 25, and 50 µM were prepared for a standard curve. The absorbance was measured at the 540 nm wavelength.

ABTS Radical Scavenging Activity Assay: The measurement of the free radical scavenging activity of MOF-808 and ascorbic acid was performed by ABTS radical cation decolorization assay. ABTS buffer was prepared by combining 7.4 mM ABTS and 7.02 mM potassium persulfate in water. This buffer was kept[in darkness at 4 °C for 12–16 h before use. And then was kept at room temperature for 30 min before starting the experiment. The absorbance was read in a microplate reader at a wavelength of 670 nm. The percentage of inhibition was calculated using the equation below.

$$\text{ABTS scavenging percent } (\%) = [\text{control } A_0 - \text{sample } A_1/\text{control } A_0] \times 100\% \quad (1)$$

where control A_0 and sample A_1 are the absorbance of ABTS without MOF-808 and ABTS with MOF-808.

DPPH Radical Scavenging Activity Assay: The free radical scavenging activity of MOF-808 was measured by using a DPPH photometric assay. MOF-808 was dissolved in DMF solvent or 0.1M KOH buffer and ascorbic acid (positive control) were reconstituted in distilled water to obtain an initial concentration of 10 mg mL^{-1} and then mixed with 0.12 mM DPPH in methanol to make a final concentration of MOF-808 and ascorbic of 1000, 800, 600, 400, 200, 100, 80, 60, 40, and 20 µg mL^{-1} in a 96-well plate. The plate was incubated at room temperature for 30 min and then checked the absorbance at 517 nm using a microplate reader. DPPH scavenging percent was calculated by following the equation below.

$$\text{DPPH scavenging percent } (\%) = [\text{control } A_0 - \text{sample } A_1/\text{control } A_0] \times 100\% \quad (2)$$

where control A_0 and sample A_1 are the absorbance of DPPH without MOF-808 and DPPH with MOF-808.

DCF-DA Assay: The estimation of ROS was performed by using raw 267.4 cells. Cells were cultured at 1.6×10^6 at 37 °C, 5% CO_2 overnight. Harvested cells and seeded at 12×10^5 cells per well in a 96-well plate for overnight. After incubation, cells were treated with different concentrations of MOF-808 (1, 10, and 100 ng mL^{-1}) for 1 h and then treated with 100 µg mL^{-1} of LPS. After 24-h incubation, the cells were washed with 1× PBS buffer and then 20 µM of DCF-DA solution was added and incubated at 37 °C, 5% CO_2 for 45 min in the dark. The fluorescence was measured using a microplate reader at 485 and 535 nm excitation and emission, respectively.

In Vitro Cell Migration Assay: NIH-3T3 cells were seeded in a 6-well plate at a density of 1.5×10^5 cells mL^{-1} and incubated in a complete medium till cell confluence reached about 80–90%. The cells were further grown for the next 20 h at 37 °C in a 5% CO_2 incubator. A uniform scratch wound was created using a 200 µL sterile pipette tip, and the wound debris was discarded by phosphate-buffer saline (PBS) washing. The scratched cells were then treated with different concentrations of MOF (0, 1, 10, and 100 ng mL^{-1}) and cultured for 5, 10, or 20 h. Coverslips were mounted onto microscope slides and an ocular micrometer was used to measure the wound distance at ten random locations along with the scratch under at 40×. The wound closure distance for each sample was determined by subtracting the average wound closure for each sample from the average initial T= 0 wound distance with data represented as average percent wound closure ± SEM. Photographs of the scratches were obtained in a Mirax Desk Scanner (Zeiss, Germany) under bright field conditions.

Formation of MOF-808 Crystals in a Hydrogel Form: 0.4 g of MOF-808 was sonicated by mixing in distilled water (194 mL) for 1 h at room temperature in a 500 mL beaker. The MOF-808 solution was dispersed for 30 min at 10 000 rpm using a homogenizer (CAT, X1740). 2 g of poly(acrylic acid) (PAA; trade name Carbomer) was added to the prepared solution and mixed for 1 h using an overhead stirrer. The weight concentrations of

MOF-808 were prepared as 0, 0.1, 0.2, 0.4, 0.6, and 0.8 wt% in PAA polymer. 0.54 g of triethanolamine (TEA) was added dropwise to the mixture and stirred with an overhead stirrer for 20 min at 1000 rpm. The mixture was mixed again with a planetary mixer at 1000 rpm. The MOF-808 crystals in a hydrogel form were prepared after 20 min.

Accelerated Aging Test: The samples were exposed to elevated temperatures to give the aging process under shortened timeframes to evaluate their physical characteristics. The accelerated aging temperature (TAA) was 50 °C and the real-time ambient shelf temperature (TRT) was 20 °C. The accelerated aging time (AAT, time in chamber) was calculated according to the Arrhenius equation and ASTM F 1980 standard guide. Each AAT was 22.8 days for 6 months of aging, 45.6 days for 1 year of aging, and 91.3 days for 2 years of aging.

$$\begin{aligned} &\text{AAF (accelerated aging factor)} = Q_{10}^{[(TAA-TRT)/10]} \ (\textit{There}, Q_{10} = 2.0) \\ &\textit{AAT (accelerated aging time)} = \textit{Desired aging time}/\textit{AAF} \end{aligned} \quad (3)$$

Measurement of NO on Cells with Hydrogel Treatment: The cell-free supernatants collected from the above step were also used for NO measurement. The Griess-modified reagent was used for measuring NO oxidation products on cells. A volume of 100 µL of the Griess-modified reagent was mixed with 100 µL of the supernatants. The mixtures were incubated at room temperature for 15 min. Nitrite standard solutions of 0, 1.6125, 3.125, 6.25, 12.5, 25, and 50 µm were prepared for a standard curve. The absorbance was measured at the 540 nm wavelength.

Measurement of TNF-α and IL-10 on Cells with Hydrogel Treatment: Except for the control well, each well was treated with hydrogel or 0.2% MOF hydrogel. The RAW264.7 cells (2.5 × 105 cells mL^{-1}) were seeded into the wells and treated with 1 µg mL^{-1} of LPS in 37 °C, 5% CO_2 incubator for 24 h. Subsequently, cell-free supernatants were collected and stored at −20 °C for cytokine assays. The concentration of TNF-α and IL-10 in the culture supernatant was measured using ELISA kits purchased from BD Biosciences and Mybiosource, SD, USA. The absorbance was measured at 450 nm using EPOCH2 microplate spectrophotometer (Agilent, CA, USA).

DCF-DA Assay on Cells with Hydrogel Treatment: Except for the control well, each well was treated with hydrogel or 0.2% MOF hydrogel. The RAW264.7 cells (12 × 10^5 cells mL^{-1}) were seeded into the wells and treated with 100 µg mL^{-1} of LPS in 37 °C, 5% CO_2 incubator for 24 h. Cells were washed with 1× PBS buffer and then 20 µM of DCF-DA solution was added and incubated at 37 °C, 5% CO_2 for 45 min in the dark. The fluorescence was measured using a microplate reader at 485 and 535 nm excitation and emission, respectively.

ABTS Radical Scavenging Activity Assay on Cells with Hydrogel Treatment: The measurement of the free radical scavenging activity of hydrogel and 0.2% MOF-808 hydrogel was performed by ABTS radical cation decolorization assay. ABTS buffer was prepared by combining 7.4 mm ABTS and 7.02 mm potassium persulfate in water. This buffer was kept in darkness at 4 °C for 12–16 h before use and then kept at room temperature for 30 min before starting the experiment. The absorbance was read in a microplate reader at a wavelength of 670 nm. The percentage of inhibition was calculated using the equation below.

$$\text{ABTS scavenging percent}\ (\%) = [\text{control } A_0 - \text{sample } A_1/\text{control } A_0] \times 100\% \quad (4)$$

where control A_0 and sample A_1 are the absorbance of ABTS without hydrogel and ABTS with hydrogel.

Rat Skin Wound Healing Experiment: Animal experiments were approved by the Institutional Animal Care and Use Committee of Seoul National University Bundang Hospital (approval number: BA1608-206/045-02). Sprague Dawley adult male rats were ordered from BioOrient Company (Seongnam, KR) that weighed between 200 and 350 g, eight weeks old, and were housed by two rats per cage. The rats were housed at a controlled temperature of 24 °C, relative humidity of 55%, and a 12-h light cycle. Rats were randomly divided into four groups of 10 rats each those with applied hydrogel (0 wt% MOF), those with applied hydrogel (0.1 wt% MOF), those with applied hydrogel (0.2 wt% MOF), and the control group without treatment. All rats were anesthetized with isoflurane, and the dorsal hair was shaved by a shaving machine. The surgical area was disinfected with Betadine. Full-thickness excisional wounds were created using 10 mm biopsy punch-modified tools in the dorsal side of the Sprague Dawley rat. The MOF-808 hydrogel was applied to cover the wound area and the wound was sealed by film every day for 10 days, while the control group received no treatment. Application of MOF-808 for rats was performed every day.

Measurement of the Wound Area: The kinetics of wound closure was treated through digital photography from days 0 to 14 after all the wound dressings were removed. Based on the photos, the areas of the wound area were measured using ImageJ software. The percentage of wound healing was calculated by the following equation.

$$\text{Percentage of wound healing}\ (\%) = (A_0 - A_n)\ /A_0 \times 100\% \quad (5)$$

where A_0 represents the original wound area after surgery, and A_n represents the wound healing area on n^{th} day after surgery. Five mice for each group were used to determine the approximate time of wound closure.

Bacterial Infection Test: *S. aureus* was cultured in LB media until OD 600 reached 0.7. The 400 µl of this bacterial culture was mixed with 12 ml of Agar LB media and poured on a Petri dish plate and then placed a 6 mm filter paper disk impregnated with MOF-808 solution and incubated at 37 °C overnight.

Histological Analysis: On days 7 and 10, after wound healing was photographed, five rats in each group were scarified and the histological analysis of the wound healing sections was investigated. The biopsied tissues were fixed with 10% formaldehyde for 24 h at 4 °C and then embedded in paraffin. The thicknesses of sections of 5 µm were prepared for further studies. The sections were stained with hematoxylin and eosin (H&E) staining for measurement of the granulation tissue thickness and the thickness of the epidermis. The sections were stained with MT staining for the measurement of collagen density. All measurements were used to calculate by ImageJ software.

Determination of Nitrite Production in Wound Lysates: Nitrite and NO oxidation products in wound lysates were determined by using the Griess-modified reagent. The wound tissues of control and different concentrations of MOF-808 groups on days 7 and 10 were homogenized in a protein extraction solution containing 1 mM PMSF, and a protein inhibitor cocktail. The tissue extract was cleared by centrifugation at 14 000 rpm for 15 min at 4 °C and then supernatant was collected and diluted 1:1 with distilled water. A mix of 100 µL of 1× Griess modified reagent and 100 µL of tissue-diluted extract was incubated at room temperature for 15 min. The absorbance was measured the wavelength at 540 nm. Nitrite standard solutions of 0, 1.6125, 3.125, 6.25, 12.5, 25 and 50 µM were prepared for a standard curve.

Determination of ROS Production in Wound Lysates: The wound tissues of control and different concentrations of the MOF group on days 7 and 10 were ground in a protein extraction solution containing 1 mM PMSF and a protein inhibitor cocktail. The protein solution was extracted by centrifugation at 14 000 rpm for 15 min at 4 °C. The collected protein supernatant was diluted 1:1 with 1× diluted buffer. A mix of 100 µL of tissue-diluted extract and 10 µL of DCFDA solution (final concentration was 20 µM) was incubated at 37 °C for 45 min in the dark. Then, the fluorescence signal was measured at excitation (485 nm)/emission (535nm) by using the SpectraMax iD3 instrument (Molecular Devices, CA, USA).

Determination of Cytokine Production in Wound Lysates: The purified proteins on days 7 and 10 were used to determine the cytokine production using an ELISA assay. The inflammatory cytokines such as MCP-1, TNF-α, IL-6, IL-8, and IL-1β were prepared by following the guidance's instructions (standard range 10–10 000, 10–10 000, 50–1000, 62.5–2000, and 10–10 000 pg mL^{-1}, respectively, BD Biosciences and Mybiosource, SD, USA). The absorbance was measured at 450 nm using an EPOCH2 microplate spectrophotometer (Agilent, CA, USA).

Statistical Analysis: Data were defined as means ± SEM. Data were analyzed by unpaired Student's *t*-test using Prism Software (USA). In our

study, all analyses were statistically significant as $p < 0.05$ (^{ns} $p \geq 0.05$, * $p < 0.05$, ** $p < 0.005$, *** $p < 0.001$).

Supporting Information

Supporting Information is available from the Wiley Online Library or from the author.

Acknowledgements

U.R. and P.N.C. contributed equally to this work. This work was supported by the National Research Foundation of Korea (NRF) grant funded by the Korean government (MSIT) (Nos. 2022R1A2B5B01001826, 2022R1A5A2021216 and 2021R1C1C2011369), Technology Innovation Program (or Industrial Strategic technology development program, No. 20015793, Nanomaterial-based flexible and stretchable sensor system for multimodal monitoring and diagnosis of Sarcopenia) funded by the Ministry of Trade, industry & Energy (MI, Korea), and the Korea Health Technology R&D Project through the Korea Health Industry Development Institute (KHIDI), funded by the Ministry of Health & Welfare, Republic of Korea (grant number: HR22C1363).

After initial online publication, K.M.C. was made a co-corresponding author on December 18, 2023.

Conflict of Interest

The authors declare no conflict of interests.

Data Availability Statement

The data that support the findings of this study are available from the corresponding author upon reasonable request.

Keywords

hydrogels, metal-organic frameworks, proinflammatory mediators, wound healing

Received: May 25, 2023
Revised: October 30, 2023
Published online:

[1] S. Barrientos, O. Stojadinovic, M. S. Golinko, H. Brem, M. Tomic-Canic, *Wound Repair Regener.* **2008**, *16*, 585.
[2] S. Werner, R. Grose, *Physiol. Rev.* **2003**, *83*, 835.
[3] D. Stan, C. Tanase, M. Avram, R. Apetrei, N.-B. Mincu, A. L. Mateescu, D. Stan, *Exp. Dermatol.* **2021**, *30*, 1218.
[4] A. Shedoeva, D. Leavesley, Z. Upton, C. Fan, *Evidence-Based Complementary Altern. Med.* **2019**, *2019*, 2684108.
[5] M. Hajialyani, D. Tewari, E. Sobarzo-Sánchez, S. M. Nabavi, M. H. Farzaei, M. Abdollahi, *Int. J. Nanomed.* **2018**, *13*, 5023.
[6] S. Saghazadeh, C. Rinoldi, M. Schot, S. S. Kashaf, F. Sharifi, E. Jalilian, K. Nuutila, G. Giatsidis, P. Mostafalu, H. Derakhshandeh, K. Yue, W. Swieszkowski, A. Memic, A. Tamayol, A. Khademhosseini, *Adv. Drug Delivery Rev.* **2018**, *127*, 138.
[7] H. N. Wilkinson, M. J. Hardman, *Open Biol.* **2020**, *10*, 200223.
[8] A. J. Whittam, Z. N. Maan, D. Duscher, V. W. Wong, J. A. Barrera, M. Januszyk, G. C. Gurtner, *Adv. Wound Care* **2016**, *5*, 79.
[9] T. Velnar, T. Bailey, V. Smrkolj, *J. Int. Med. Res.* **2009**, *37*, 1528.
[10] M. Mittal, M. R. Siddiqui, K. Tran, S. P. Reddy, A. B. Malik, *Antioxid. Redox Signaling* **2014**, *20*, 1126.
[11] D. Miricescu, S. C. Badoiu, I.-I. Stanescu-Spinu, A. R. Totan, C. Stefani, M. Greabu, *Int. J. Mol. Sci.* **2021**, *22*, 9512.
[12] N. N. Houreld, P. R. Sekhejane, H. Abrahamse, *Lasers Surg. Med.* **2010**, *42*, 494.
[13] M. Rizk, M. B. Witte, A. Barbul, *World J. Surg.* **2004**, *28*, 301.
[14] A. Schwentker, Y. Vodovotz, R. Weller, T. R. Billiar, *Nitric Oxide* **2002**, *7*, 1.
[15] N. Bryan, H. Ahswin, N. Smart, Y. Bayon, S. Wohlert, J. Hunt, *Eur. Cells Mater.* **2012**, *24*, 249.
[16] C. Dunnill, T. Patton, J. Brennan, J. Barrett, M. Dryden, J. Cooke, D. Leaper, N. T. Georgopoulos, *Int. Wound J.* **2017**, *14*, 89.
[17] M. Gouzos, M. Ramezanpour, A. Bassiouni, A. J. Psaltis, P. J. Wormald, S. Vreugde, *Front. Cell. Infect. Microb.* **2020**, *10*, 110.
[18] G. Sandri, M. C. Bonferoni, S. Rossi, F. Ferrari, C. Aguzzi, C. Viseras, C. Caramella, in, *Wound Healing Biomaterials*, (Ed: M. S. Ågren), Vol. *2*, Woodhead Publishing, UK **2016**, Ch. 19.
[19] F. García-Villén, I. M. S. Souza, R. De Melo Barbosa, A. Borrego-Sánchez, R. Sánchez-Espejo, S. Ojeda-Riascos, C. V. Iborra, *Curr. Pharm. Des.* **2020**, *26*, 621.
[20] H.-C. Zhou, J. R. Long, O. M. Yaghi, *Chem. Rev.* **2012**, *112*, 673.
[21] S. Yuan, L. Feng, K. Wang, J. Pang, M. Bosch, C. Lollar, Y. Sun, J. Qin, X. Yang, P. Zhang, Q. Wang, L. Zou, Y. Zhang, L. Zhang, Y. Fang, J. Li, H.-C. Zhou, *Adv. Mater.* **2018**, *30*, 1704303.
[22] N. Stock, S. Biswas, *Chem. Rev.* **2012**, *112*, 933.
[23] J. E. Efome, D. Rana, T. Matsuura, C. Q. Lan, *J. Mater. Chem. A* **2018**, *6*, 4550.
[24] X. Liu, X. Wang, F. Kapteijn, *Chem. Rev.* **2020**, *120*, 8303.
[25] X. T. Liu, B. B. Qian, D. S. Zhang, M. H. Yu, Z. Chang, X. H. Bu, *Coord. Chem. Rev.* **2023**, *476*, 214921.
[26] I. Erucar, T. A. Manz, S. Keskin, *Mol. Simul.* **2014**, *40*, 557.
[27] N.-Y. Huang, H. He, S. Liu, H.-L. Zhu, Y.-J. Li, J. Xu, J.-R. Huang, X. Wang, P.-Q. Liao, X.-M. Chen, *J. Am. Chem. Soc.* **2021**, *143*, 17424.
[28] J. Yoo, U. Ryu, W. Kwon, K. M. Choi, *Sens. Actuators, B* **2019**, *283*, 426.
[29] R. V. Pinto, S. Wang, S. R. Tavares, J. Pires, F. Antunes, A. Vimont, G. Clet, M. Daturi, G. Maurin, C. Serre, M. L. Pinto, *Angew. Chem., Int. Ed.* **2020**, *59*, 5135.
[30] J. Zhuang, A. P. Young, C.-K. Tsung, *Small* **2017**, *13*, 1700880.
[31] S. Chen, J. Lu, T. You, D. Sun, *Coord. Chem. Rev.* **2021**, *439*, 213929.
[32] M. Yin, J. Wu, M. Deng, P. Wang, G. Ji, M. Wang, C. Zhou, N. T. Blum, W. Zhang, H. Shi, N. Jia, X. Wang, P. Huang, *ACS Nano* **2021**, *15*, 17842.
[33] S. Yao, J. Chi, Y. Wang, Y. Zhao, Y. Luo, Y. Wang, *Adv. Healthcare Mater.* **2021**, *10*, 2100056.
[34] L. Zhang, Z. Liu, Q. Deng, Y. Sang, K. Dong, J. Ren, X. Qu, *Angew. Chem., Int. Ed.* **2021**, *60*, 3469.
[35] J. Li, L. Liu, Y. Ai, Y. Liu, H. Sun, Q. Liang, *ACS Appl. Mater. Interfaces* **2020**, *12*, 5500.
[36] Y. Chen, J. Cai, D. Liu, S. Liu, D. Lei, L. Zheng, Q. Wei, M. Gao, *Regener. Biomater.* **2022**, *9*, rbac019.
[37] E. Caló, V. V. Khutoryanskiy, *Eur. Polym. J.* **2015**, *65*, 252.
[38] L. Wang, L. Duan, G. Liu, J. Sun, M.-A. Shahbazi, S. C. Kundu, R. L. Reis, B. Xiao, X. Yang, *Adv. Sci.* **2023**, *10*, 2207352.
[39] M. Fu, X. Deng, S.-Q. Wang, F. Yang, L.-C. Lin, M. J. Zaworotko, Y. Dong, *Sep. Purif. Technol.* **2022**, *288*, 120620.
[40] H. Furukawa, F. Gándara, Y.-B. Zhang, J. Jiang, W. L. Queen, M. R. Hudson, O. M. Yaghi, *J. Am. Chem. Soc.* **2014**, *136*, 4369.
[41] H.-Q. Zheng, C.-Y. Liu, X.-Y. Zeng, J. Chen, J. Lü, R.-G. Lin, R. Cao, Z.-J. Lin, J.-W. Su, *Inorg. Chem.* **2018**, *57*, 9096.
[42] C. Ardila-Suárez, J. Rodríguez-Pereira, V. G. Baldovino-Medrano, G. E. Ramírez-Caballero, *CrystEngComm* **2019**, *21*, 1407.

[43] E. Aunan, C. W. Affolter, U. Olsbye, K. P. Lillerud, *Chem. Mater.* **2021**, *33*, 1471.
[44] P.-H. Chang, C.-Y. Chen, R. Mukhopadhyay, W. Chen, Y.-M. Tzou, B. Sarkar, *J. Colloid Interface Sci.* **2022**, *623*, 627.
[45] J. Jiang, F. Gándara, Y.-B. Zhang, K. Na, O. M. Yaghi, W. G. Klemperer, *J. Am. Chem. Soc.* **2014**, *136*, 12844.
[46] T.-T. Li, Y.-M. Liu, T. Wang, Y.-L. Wu, Y.-L. He, R. Yang, S.-R. Zheng, *Microporous Mesoporous Mater.* **2018**, *272*, 101.
[47] Y. Peng, H. Huang, Y. Zhang, C. Kang, S. Chen, L. Song, D. Liu, C. Zhong, *Nat. Commun.* **2018**, *9*, 187.
[48] H. G. T. Ly, G. Fu, A. Kondinski, B. Bueken, D. De Vos, T. N. Parac-Vogt, *J. Am. Chem. Soc.* **2018**, *140*, 6325.
[49] M. B. Witte, A. Barbul, *Am. J. Surg.* **2002**, *183*, 406.
[50] B. Xiao, P. S. Wheatley, X. Zhao, A. J. Fletcher, S. Fox, A. G. Rossi, I. L. Megson, S. Bordiga, L. Regli, K. M. Thomas, R. E. Morris, *J. Am. Chem. Soc.* **2007**, *129*, 1203.
[51] J. Baek, B. Rungtaweevoranit, X. Pei, M. Park, S. C. Fakra, Y.-S. Liu, R. Matheu, S. A. Alshmimri, S. Alshehri, C. A. Trickett, G. A. Somorjai, O. M. Yaghi, *J. Am. Chem. Soc.* **2018**, *140*, 18208.
[52] S. Ranganath, A. Bhandari, N. Avitahl-Curtis, J. Mcmahon, D. Wachtel, J. Zhang, C. Leitheiser, S. G. Bernier, G. Liu, T. T. Tran, H. Celino, J. Tobin, J. Jung, H. Zhao, K. E. Glen, C. Graul, A. Griffin, W. C. Schairer, C. Higgins, T. L. Reza, E. Mowe, S. Rivers, S. Scott, A. Monreal, C. Shea, G. Bourne, C. Coons, A. Smith, K. Tang, R. A. Mandyam, et al., *PLoS One* **2015**, *10*, 0141330.
[53] L. Litov, P. Petkov, M. Rangelov, N. Ilieva, E. Lilkova, N. Todorova, E. Krachmarova, K. Malinova, A. Gospodinov, R. Hristova, I. Ivanov, G. Nacheva, *Int. J. Mol. Sci.* **2021**, *22*, 10730.
[54] A. Tuxpan-Pérez, M. A. Ibarra-Valencia, B. E. Estrada, H. Clement, L. L. Corrales-García, G. P. Espino-Solis, G. Corzo, *Antibiotics* **2022**, *11*, 607.
[55] M. Monteleone, A. C. Stanley, K. W. Chen, D. L. Brown, J. S. Bezbradica, J. B. Von Pein, C. L. Holley, D. Boucher, M. R. Shakespear, R. Kapetanovic, V. Rolfes, M. J. Sweet, J. L. Stow, K. Schroder, *Cell Rep.* **2018**, *24*, 1425.
[56] C. Rébé, F. Ghiringhelli, *Cancers* **2020**, *12*, 1791.
[57] R. L. Hassfurther, P. C. Canning, R. W. Geib, *Vet. Immunol. Immunopathol.* **1994**, *42*, 117.
[58] T. Ahlstrand, L. Kovesjoki, T. Maula, J. Oscarsson, R. Ihalin, *J. Oral Microbiol.* **2019**, *11*, 1549931.
[59] H. Andrade, W. Lin, Y. Zhang, *J. Biol. Chem.* **2019**, *294*, 6397.
[60] S. Daliran, M. Ghazagh-Miri, A. R. Oveisi, M. Khajeh, S. Navalón, M. Âlvaro, M. Ghaffari-Moghaddam, H. Samareh Delarami, H. García, *ACS Appl. Mater. Interfaces* **2020**, *12*, 25221.
[61] V. K. Shukla, D. Shukla, S. K. Tiwary, S. Agrawal, A. Rastogi, *J. Wound Care* **2007**, *16*, 291.
[62] A. Poddar, S. Pyreddy, S. A. Polash, C. M. Doherty, R. Shukla, *Biomater. Biosyst.* **2022**, *8*, 100065.
[63] A. Jakovija, T. Chtanova, *Front. Immunol.* **2023**, *14*, 1060258.
[64] N. Lohmann, L. Schirmer, P. Atallah, E. Wandel, R. A. Ferrer, C. Werner, J. C. Simon, S. Franz, U. Freudenberg, *Sci. Transl. Med.* **2017**, *9*, aai9044.
[65] J.-M. Lü, P. H. Lin, Q. Yao, C. Chen, *J. Cell. Mol. Med.* **2010**, *14*, 840.
[66] E. Di Giuseppe, F. Corbi, F. Funiciello, A. Massmeyer, T. N. Santimano, M. Rosenau, A. Davaille, *Tectonophysics* **2015**, *642*, 29.
[67] I. Romero-Muñiz, C. Romero-Muñiz, I. Del Castillo-Velilla, C. Marini, S. Calero, F. Zamora, A. E. Platero-Prats, *ACS Appl. Mater. Interfaces* **2022**, *14*, 27040.
[68] A. C. D. O. Gonzalez, T. F. Costa, Z. D. A. Andrade, A. R. A. P. Medrado, *An. Bras. Dermatol.* **2016**, *91*, 614.
[69] A. Desmouliere, I. A. Darby, B. Laverdet, F. Bonté, *Clin., Cosmet. Invest. Dermatol.* **2014**, *7*, 301.
[70] M. Rodrigues, N. Kosaric, C. A. Bonham, G. C. Gurtner, *Physiol. Rev.* **2018**, *99*, 665.
[71] R. Guillamat-Prats, *Cells* **2021**, *10*, 1729.
[72] V. Prabhu, B. S. S. Rao, A. C. K. Rao, K. Prasad, K. K. Mahato, *Lasers Med. Sci.* **2022**, *37*, 171.
[73] M. Abate, S. Pisanti, M. Caputo, M. Citro, C. Vecchione, R. Martinelli, *Int. J. Mol. Sci.* **2020**, *21*, 3657.